Nanotechnology

Surface nanostructuring of alkali-aluminosilicate gorilla display glass substrates using a maskless process

To cite this article before publication: Rongtao Cao *et al* 2022 *Nanotechnology* in press https://doi.org/10.1088/1361-6528/ac5a81

IOP Publishing Journal Title
Journal **XX** (XXXX) XXXXXX https://doi.org/XXXX/XXXX

Surface Nanostructuring of Alkali-Aluminosilicate Gorilla Display Glass Substrates Using a Maskless Process

Rongtao Cao[1], Ziyu Zhou[5], Sajad Haghanifar[2], Jingyu Wu[1], Ming-Jun Li[3], Susheng Tan[1,4], Paul W. Leu[2,5] and Kevin P. Chen[1]*

[1]Department of Electrical and Computer Engineering, University of Pittsburgh, Pittsburgh, Pennsylvania, 15261, USA
[2]Department of Industrial Engineering, University of Pittsburgh, Pittsburgh, Pennsylvania 15261, USA
[3]Corning Incorporated, Corning, New York, 14831, USA
[4]Petersen Institute of NanoScience and Engineering, University of Pittsburgh, Pittsburgh, PA 15261, USA
[5]Department of Mechanical Engineering and Materials Science, University of Pittsburgh, Pittsburgh, PA 15261, USA

E-mail: pec9@pitt.edu

Abstract

This paper reports on the formation of moth-eye nanopillar structures on surfaces of alkali-aluminosilicate Gorilla glass substrates using a self-masking plasma etching method. Surface and cross-section chemical compositions studies were carried out to study the formation of the nanostructures. CF_x induced polymers were shown to be the self-masking material during plasma etching. The nanostructures enhance transmission at wavelengths over 525 nm and may be utilized for fluid-induced switchable haze. Additional functionalities associated with nanostructures may be realized such as self-cleaning, anti-fogging, and stain-resistance.

Keywords: Subwavelength structures, Optical properties, Nanostructure fabrication, Optical switching devices

1. Introduction

Silica glass is the most widely used optical material for modern technologies including displays, solar modules, optical waveguides, and lighting. Surface nanostructuring and composition tempering of silica glass substrates have been subject to intense research and development works to enhance the optical and mechanic performance of glass substrates [1].

Over the last two decades, various surface nanostructuring schemes have also been studied to change the physical morphology and material properties of glass substrates for solar energy applications. Fabrication of nanostructures on glass substrates with appropriate sizes and geometries have been reported to exhibit interesting optical properties such as haze or antireflection at visible and near infrared wavelength ranges for optical applications such as photovoltaic solar cells, optical detectors, and light emitting diodes [2-5]. Ion-assisted film deposition [6] and nanoimprint methods [7] have been reported to form nanostructures on silica glass substrates to produce antireflective surface structures. However, these approaches involve deposition and nanoimprinting of additional materials on the surface of silica glasses with mismatched thermal expansion coefficients, which undermine the long-term stability and performance under temperature change [8, 9]. Another commonly used approach is to utilize a sacrificial layer as a mask followed by the plasma etching to form the antireflective or haze structures directly into glass surfaces. Commonly used sacrificial masks include metal nanoparticles created by thermal annealing of thin metal film [2, 9, 10]. Self-assembled polymer spheres have also been

demonstrated as sacrificial masks [11]. These processes often involve multiple fabrication steps including sacrificial layer depositions, thermal annealing, followed by plasma etching processing and post fabrication cleaning. The multiple steps involved in various masked approaches are costly and often negate comparative advantages of nanostructures versus conventionally multi-layer antireflective coating schemes.

Recently, maskless processes have been reported to produce functional nanostructures on surfaces of fused silica and fused quartz substrates with a single step of reactive ion etching (RIE) process [12-16]. This is a much simpler process than those involving multi fabrication steps using various mask schemes. Through tuning of processing parameters [12, 13] and tempering of composition of fused silica [14], high aspect ratio nanostructures can be formed directly on silica surfaces to exhibit broadband anti-reflection characteristics [12, 14] or strong scattering characteristics (haze) [13, 17] for solar energy and lighting applications. However, most successful demonstrations of these maskless processing schemes have been on a very small group of silica glass materials including pure fused silica (SiO_2) and a dopant variant of fused silica. This severely limits applications of the maskless processing techniques.

This paper studies the maskless plasma process to produce nanostructures on Alkali-aluminosilicate, also known as Gorilla glass. Gorilla glass is a low-cost glass that uses ion exchange to improve the mechanical strength of the material and used far more pervasively than fused silica for applications such as displays and solar energy applications. As the mechanical integrity of amorphous silica glass substrates are prone to surface defect, formation of nanostructures in chemically strengthened layer of Gorilla glass can also effectively mitigate the impacts of defects formed by RIE processes on the mechanical integrity of glass substrates. In this paper, we report on the creation of moth-eye like structures covered with nano-pillars to enhance the gorilla glass transmittance through a maskless process. The processed surface is surperhydrophilic and demonstrates the ability to change haze depending on water coverage, which may be used as "smart glass" [14].

2. Experimental

Gorilla glass wafers (Valley Supplied, 1 mm thick) and fused silica (UniversityWafer, 180 μm) were cleaned in acetone, isopropyl alcohol, deionized water ultrasonic bath for 20 min, respectively, and then dried by N_2 flow. The glass wafer was then transferred into a Phantom RIE system with a 5-inch silicon protected chamber chunk. The maskless etching process [12] was carried out utilizing a mixture gas of SF_6 (10 sccm), CHF_3 (40 sccm), and inert Ar (80 sccm). The etching radio frequency power and pressure were optimized to be 280 W and 200 mTorr, respectively. The etching time ranged from 0.5 h to 5 h for gorilla glass and 10 min to 50 min for fused silica.

To evaluate the surface and cross-section morphology, Zeiss Sigma 500VP scanning electron microscope (SEM) with an optimized accelerating voltage of 3 kV was employed. A thin layer of Au-Pd was deposited on the sample by a sputter coater (Hummer) before imaging. The element composition measurement was performed by an Oxford Instruments AZtecenergy-dispersive X-ray spectroscopy (EDX) system attached to the Zeiss Sigma 500VP SEM. A lambda 750 spectrophotometer (PerkinElmer) was used to measure the reflectance and total transmittance spectra over the wavelength range of 300 to 800 nm. An 8-degree tilt wedge was also inserted in the optical path in order to collect the reflected light. Finally, wetting characterization was evaluated by means of VCA 2000 video contact angle goniometer. A volume of 2 μl distill water droplet was placed on the sample surface and the contact angle was automatically calculated by the software.

3. Results and discussion

Imaged by a SEM, figures 1(a-c) shows both top views and zoomed-in cross-sections of nanostructures formed on surface of Gorilla glass substrate as a function of plasma etching times. After 0.5-hour etching, moth-eye like structures with an average height of 500-nm were formed on the surface as shown in figure 1(a). The top diameter of the fabricated nanostructures is less than 100 nm, although is relatively large compared with recent literatures with plasma dry etching approach [18-20], still can be considered in the nanoscale. These nanostructures are randomly distributed on the surface and cover approximated 50% of surface area. With increased etching time, these nanostructures merge together to cover more surface area. The moth-eye structures grow sharper and form cone-like structures. The heights of these cone-like structures grew to 3-μm after 3-hour etching times and then decreases to 2 μm after 5-hour etching times. The etch rate increases from 0.8 μm/h to 1 μm/h for the first 1.5 h and then decreases to 0.7 μm/h after 3 h. The same recipe was also applied on pure silica substrate and the results are shown in figure 1(d).

The morphology shown in figure 1(a-c) is significantly different from the nanostructures formed on fused silica as shown in figure 1(d) after 50-minute etching. The same plasma etching receipts results in densely packed "nano-grass" structures. The diameters of nano-column formed on the surface of fused silica do not change across the entire nano-pillar as shown in figure 1(d). This dramatically different surface morphology could be due to the different compositions of two glass samples. More importantly, the formation of cone-like surface structures could be due to the non-uniform glass composition in chemically strengthened layer of Gorilla glass, where Na+ is replaced by Ca+, which results in a different plasma etching rate. This suggests that through tempering of the chemical compositions of glass substrates using various fabrication processes such as ion implantation, ion-diffusion, or ion exchange, it is possible to control shape, size, and morphology of this maskless etching process.

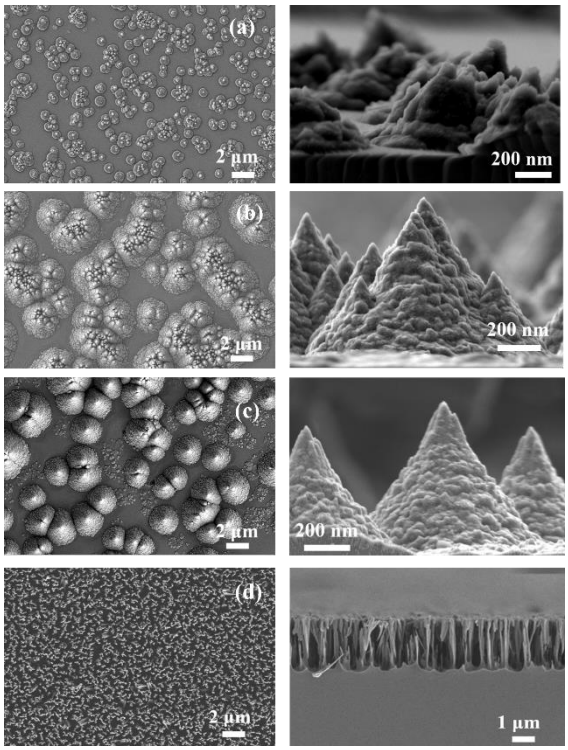

Figure 1. SEM photos showing top and side views of surface morphology of Gorilla glass after (a) 0.5-hour, (b) 3-hour, and (c) 5-hour etching. (d) Surface morphology of fused silica after 50-minute etching using the same conditions.

Figure 2 shows the etched height of the structures and their surface coverage on gorilla glass when exposed to

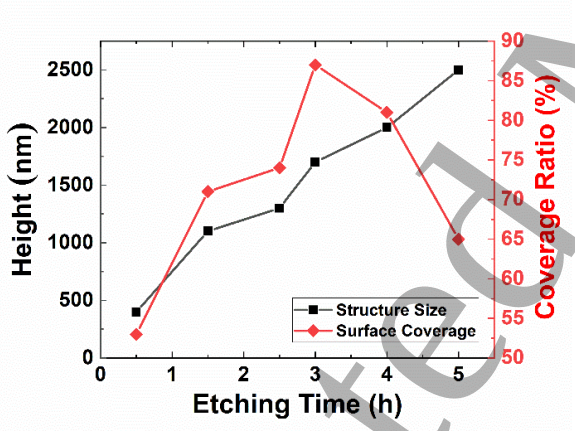

Figure 2. The etched structure height and surface coverage in response to various etching time.

plasma for various etching times. It is noted that the height of the etched structural is proportional to the etching time. An initial increase of the surface coverage of the structure from 53% to 87% was obtained when the etching time is increased to 3 h. Further etching beyond 3h, on the other hand, reduces the surface coverage (figure 1(c)). The initial increase of the coverage ratio is due to the generation of $(CF_2)_n$ radicals forming the polymer films on the surface. As etching continues, the formed structure acts as the mask for the following etching. Meanwhile the plasma has been scattered due to the high coverage of the etched structures so that it is hard to reach the surface of the glass. However, it continues to etch the small structures on the cones even with a slow speed. As a result, the coverage decreases.

The Gorilla glass is made up of aluminosilicate composed of SiO_2, Al_2O_3, MgO, Na_2O, CaO, and others. During the fusion manufacturing process, the molten glass fuses together to form a continuous sheet of flat glass [21]. When etchant gasses are introduced during the reactive etching, the gas CHF_3 is dissociated into free radicals or ions and reacts with the oxides forming metal fluorides. Meanwhile some CF_2 radicals or ions form polymer films on the glass surface; those polymer films act as a mask during the etching process. A simplified scheme for the CHF_3 dissociation and further reaction with the Gorilla glass is shown below:

$$CHF_3 \rightarrow CF_2 + F + H$$

$$SiO_2 + 4F \rightarrow SiF_4 + O_2$$

$$nCF_2 \rightarrow (CF_2)_n$$

$$2Al_2O_3 + 12\,F \rightarrow 4AlF_3 + 3O_2$$

$$2MgO + 4F \rightarrow 2MgF_2 + O_2$$

$$2CaO + 4F \rightarrow 2CaF_2 + O_2$$

$$2Na_2O + 4F \rightarrow 4NaF + O_2$$

This hypothesis is confirmed by the surface elemental composition maps measured by SEM in energy-dispersive X-ray (EDX) mode. The results are illustrated in figure 3. A large amount of F and Na elements were detected, which indicates the high density of NaF and $(CF_2)_n$ coverage on the surface [13]. The C peak located at 0.3 keV was also detected by EDX, which further confirmed the presence of CF and CF_2 radicals. These radicals have been shown to be a crucial component for the C-F polymer formation acting as a mask for the etching process [12, 22]. In the mapping, Si and O atoms increase gradually from the tip to the bottom of the substrate. The lack of those two elements on the tip can be explained by the boiling point of generated SiF_4 and OF_2 compound. The boiling point for SiF_4 and OF_2 are -86 ^oC and -144 ^oC, which cannot survive the heat generated during the etching process.

Compared with Si and O, elements such as Al, Mg, Ca are more uniformly distributed within the whole structure. The existence of those elements at the tip of the structure can be attributed to the formation of high boiling point compound of MgF_2, AlF_3, and CaF_2 (over 1000 ^oC). A.J.van Rooosmalen reported that nonvolatile metal fluorides such as NaF, MgF_2, AlF_3, and CaF_2 can act as chain initiator for the polymer growth [23], which explains the large quantity of Mg, Al, Ca on the structure surface. The MgF_2, AlF_3, and CaF_2 solid compounds formed during the reactive etching processes form

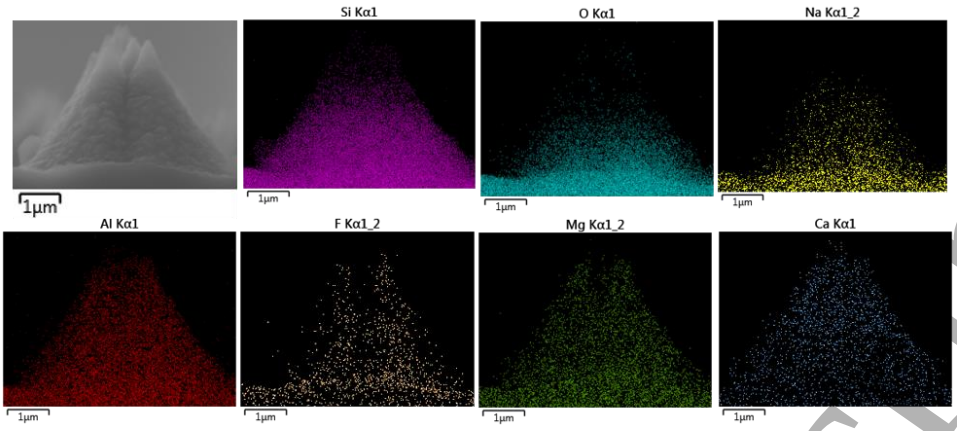

Figure 3. SEM-EDX spectra of cross-section composition

islands acting as masks resulting in the formation of corn-shaped surface structures.

Figure 4(a) shows the total transmittance spectra of the samples with various etching times. Compared with bare gorilla glass, the sample with 0.5 h etching shows enhanced transmittance beyond 525 nm. This can be attributed to the well-studied moth eye effect that the nanometer scale moth-eye on the glass, which creates a continuous graded refractive index distribution between the glass substrate and air [24]. As the plasma etching continues, the nanoscale moth-eye structures evolve into microscale structures, resulting in significantly increased scattering and reduction in light transmittance at wavelengths less than 570 nm [2]. Hoshii also confirmed in his publication that the generated NaF crystals also contributes to this observation by acting as the residual light scatter on the surface [25]. However, a slightly increased transmittance is observed for 1.5, 3, and 5 h etched substrates at longer wavelengths above 570 nm. This transmittance behavior is due to the influence of the surface structure shapes on transmittance compared with scattering. As shown in figure 1, with increasing etch time, moth-eye structures turn into multi-cone structures and finally form single cone structures, generating a more shaper structure that provides a more graded index distribution between air and glass substrate [11].

Unlike the transmittance, the reflectance continuously decreases with increased etching time was observed in figure 4(b). The reflectance drops to around 6.2% after 5 h etching. This is the result of graded index change resulted from structure shape and size. To further enhance the transmittance and depress the reflectance, double side etching, instead of one, would be beneficial. Metal species such as Mg, Al, and Ca may deposit on the surface resulting in some absorption as well.

Based on the gorilla glass shapes obtained under various plasma etch times in figure 1, the reflection property of different nanocone shapes was investigated by solving Maxwell's equations using the finite difference time domain (FDTD) method [26, 27]. The optical constant (refractive index) of gorilla glass was calculated from the experimental measurements of planar gorilla glass, shown in figure 4(a). Periodic boundary conditions were utilized to demonstrate the periodic distributed nanocone arrays. Perfectly matched layer (PML) boundary conditions were used for the top and bottom of the simulation cell [28]. An auto non-uniform meshing was applied throughout the simulation region. The truncated nanocone arrays were defined by four parameters: (1) pitch of the arrays α, (2) top diameter D_{top}, (3) bottom diameter D_{bot} and (4) height H. Similar shape geometries were picked out and compared to experimental measurement of reflection.

Figure 4(b) demonstrated the plots of the simulated and measured reflectance spectrum dependent on the wavelength for the gorilla glass with different etch times: (a) 0.5h, (b) 1.5h, (c) 3h, and (d) 5h. Within the whole visible light range, the computational results reasonably agree to the experimental measurements. The relative larger variation (0.4%) for 3h etching sample results from the approximation of some smaller nanocone geometry. As illustrated in right image in figure 1(b), some small cones were approximated, thus introducing some variations. Modulated reflectivity spetrum was also observed for the simulated structures, which is due to the fact that the simulated structures are semi-infinite. The repeating structures can have some constructive and destructive interference at various wavelengths, resulting in some peaks and valleys in the simulated reflection spectra. The experimentally fabricated structures have much more disorder, so these effects are not presented in measured reflection spectra. Compared with more UV transparent graphene [29] suitable for electrode material, the less transparent and more reflective gorilla glass had been used as the optical waveguide material [30] through fs-laser inscription process [31-32]. Meanwhile, after ion-exchange process, the strength of gorilla glass has been significantly enhanced and has been widely utilized as the protective phone

screen. Thus, the nanostructuring of the gorilla glass could provide enhanced functionality of the gorilla glass.

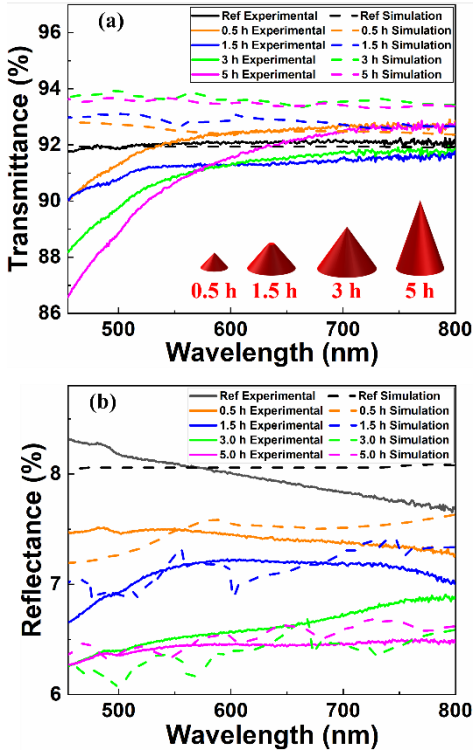

Figure 4. (a) Simulated and measured transmittance spectra of the sample, inset are the model structures utilized in simulation. (b) Simulated and measured reflectance spectra of the sample.

The wetting property was characterized by the water contact angle. Figure 5 shows the comparison of a droplet on bare glass, glass after etching, and etched glass after deionized water rinsing. According to Wenzel's model [33],

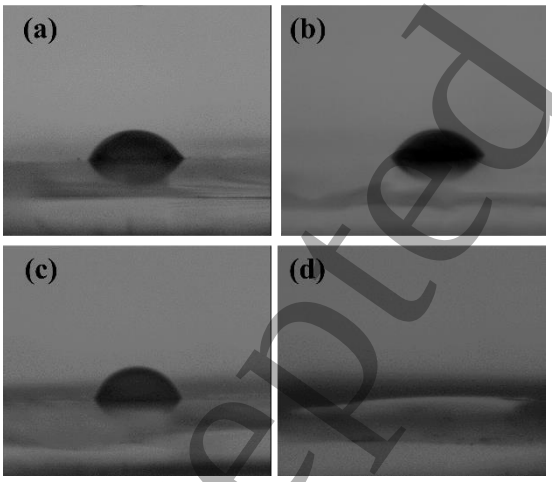

Figure 5. Wetting property of (a) bare glass. (b) 3 h etched sample before cleaning. (c) 5 h etched sample before cleaning. (d) 5 h etched sample after cleaning.

glass wetting characteristic is proportion to its surface roughness r. With the increased cone height and size, the surface roughness should increase accordingly, resulting in a decreased contact angle and improved hydrophilic property. However, a more hydrophobic surface was obtained after plasma etching. This disappears after deionized water cleaning, meaning the surface topography cannot account for the change in surface wetting alone. L.K Verma [2] already demonstrated the significant effects of surface chemistry composition on wetting property: a very thin layer of metal coating on top of the surface can alter the surface wetting characteristic dramatically. Di Mundo [34] has reported that a rising ratio of F to C can alternate the surface chemistry and increase the hydrophobic of the etched surface. This may account for the contact angle change before and after cleaning the etched sample surface. As shown in the table 1, the F element was significantly removed from the sample surface after cleaning, which dramatically lower the F to C ratio and helps to recover the hydrophilic property of the etched sample. The nanostructures could potentially be functionalized to be superhydrophobic and realize functionalities such as self-cleaning, anti-fogging, and stain resistance.

Table 1. Surface chemical composition

Chemical Composition (Wt%)	F	O	C	Si	Mg	Al	Na
Without Etching	-	46	12	35.5	0.28	2.7	1.7
Before Surface Cleaning	43.8	7.5	6.8	4.8	8.9	10.3	13.4
After Surface Cleaning	8.5	30.5	-	16.9	5.1	18.6	8.4

Figure 6 shows the transition of high haze to low haze surface when dropping the water on the long-time processed surface, which is a reversible process. This is a result of the smaller mismatch of refractive indices of the water-gorilla glass [35]. Due to the super hydrophilicity of glass, water cover the whole sample surface, which creates a water-glass interface instead of air-glass and reduces the refractive index mismatch between those interfaces, resulting in lower haze.

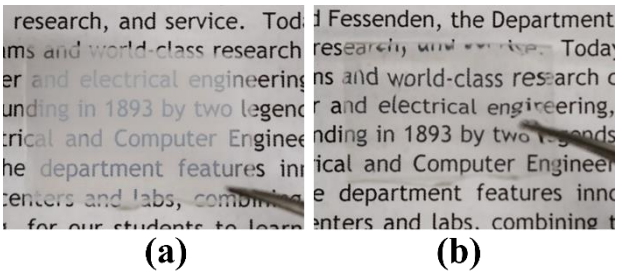

Figure 6. Optical image of the etched gorilla glass (a) without and (b) with water coverage.

4. Conclusion

In summary, moth-eye structures were fabricated on gorilla glass with one step maskless RIE. Antireflective surfaces were achieved after 0.5 h etching. With continued etching, the moth-eye structures turn into sharp cone shapes. Surface and cross-section composition confirm a CF_x based polymer mask layer. After cleaning the sample surface, enhanced hydrophilicity was realized. The CF_x mask layer results in a hydrophobic surface before cleaning. Finally, a haze switchable surface was obtained after long time etching. The ability to etch nanostructures into Gorilla glass may enable other functionalities associated with nanostructures such as self-cleaning, anti-fogging, and stain-resistance.

Acknowledgements

The author would like to acknowledge the financial support from Pennsylvania Department of Community and Economic Development (DCED) state contract C000072548.

Confilict of interest

The author decleares no confilct of interest.

References

[1] Haghanifar S, Galante A J and Leu P W 2020 *ACS nano* **14** 16241
[2] Verma L K, Sakhuja M, Son J, Danner A, Yang H, Zeng H and Bhatia C 2011 *Renewable Energy* **36** 2489
[3] Lee C, Bae S Y, Mobasser S and Manohara H 2005 *Nano Lett.* **5** 2438
[4] Cao R, Wu J, Liang G, Ohodnicki P R and Chen K P 2019 *IEEE Sens. J.* **20** 1922
[5] Cao R, Ding H, Kim K-J, Peng Z, Wu J, Culp J T, Ohodnicki P R, Beckman E, Chen K P 2020 *Sens. and Actuators*, B **324** 128627
[6] Liou Y Y, Kuo L H, Yan J Y and Jaing C C 2012 *Jpn. J. Appl. Phys*. **51** 042501
[7] Bae B-J, Hong S-H, Hong E-J, Lee H and Jung G-y 2009 *Jpn. J. Appl. Phys*. **48** 010207
[8] Lalanne P and Morris G M 1996 In *Developments in Optical Component Coatings* **2776** 300
[9] Leem J W, Yeh Y and Yu J S 2012 *Opt. Express* **20** 4056
[10] Infante D, Koch K W, Mazumder P, Tian L, Carrilero A, Tulli D, Baker D and Pruneri V 2013 *Nano Res.* **6** 429
[11] Ji S, Song K, Nguyen T B, Kim N and Lim H 2013 *ACS Appl. Mater. Interfaces* **5** 10731
[12] Ye X, Jiang X, Huang J, Geng F, Sun L, Zu X, Wu W and Zheng W 2015 *Sci. Rep*. **5** 1
[13] Haghanifar S, Gao T, De Vecchis R T R, Pafchek B, Jacobs T D and Leu P W 2017 *Optica* **4** 1522
[14] Gong X, Li J, Chen S and Wen W 2009 *Appl. Phys. Lett*. **95** 251907
[15] Haghanifar S, McCourt M, Cheng B, Wuenschell J, Ohodnicki P and Leu P W 2019 *Mater. Horiz*. **6** 1632
[16] Haghanifar S, McCourt M, Cheng B, Wuenschell J, Ohodnicki P and Leu P W 2020 *Optica* **7** 784
[17] Haghanifar S, Lu P, Kayes M I, Tan S, Kim K-J, Gao T, Ohodnicki P and Leu P W 2018 *J. Mater. Chem. C* **6** 9191
[18] Lin Y, Yuan R, Zhou C, Dong Z, Su Z, Zhang H, Chen Z, Li Y and Wang C 2020 *Nanotechnology* **31** 315301
[19] Chang B 2019 *Nanotechnology* **31** 085301
[20] Anam M K and Ahn E C 2019 *Nanotechnology* **30** 495202
[21] Welch R C, Smith J R, Potuzak M, Guo X, Bowden B F, Kiczenski T, Allan D C, King E A, Ellison A J and Mauro J C 2013 *Phys. Rev. Lett.* **110** 265901
[22] Booth J, Cunge G, Chabert P and Sadeghi N 1999 *J. Appl. Phys*. **85** 3097
[23] Roosmalen A V 1984 *Vaccum* **34** 429.
[24] Clapham P and Hutley M 1973 *Nature* **244** 281
[25] Hoshii T, Tamaki R, Watanabe K, Sugiyama M, Okada Y and Miyano K 2016 *J. Opt.* **18** 064008
[26] Yee K 1966 *IEEE Transactions on Antennas and Propagation*, **14** 302
[27] Taflove A 1980 *IEEE Transactions on electromagnetic compatibilit* **3** 191
[28] Bérenger J-P 2007 *Synthesis Lectures on Computational Electromagnetics* **2** 1
[29] Lin G, Lin Y and Sun B 2021 *Nanotechnology* **33** 085204
[30] Almeida G F, Almeida J M, Martins R J, De Boni L, Arnold C B and Mendonca C R 2017 *Laser Phys*. **28** 015401
[31] Huang S, Wang M, Huang Y, Cao R, Li S, Zou R, Yan A, Li M and Chen K P 2017 *Conference on Lasers and Electro-Optics* 1
[32] Cao R, Yang Y, Wang M, Yi X, Wu J, Huang S and Chen K P 2020 *Optics Lett*. **45** 3163
[33] Wenzel R N 1936 *Ind. Eng. Chem*. **28** 988
[34] Di Mundo R, Palumbo F and d'Agostino R 2010 *Langmuir* **26** 5196
[35] Daimon M and Masumura A 2007 *Appl. Opt*. **46** 3811